Eur Biophys J (2018) 47:151–164
https://doi.org/10.1007/s00249-017-1237-3

ORIGINAL ARTICLE

EBSA
Biophysics in Europe

Membrane phase transition during heating and cooling: molecular insight into reversible melting

Liping Sun[1] · **Rainer A. Böckmann**[1]

Received: 4 May 2017 / Revised: 18 June 2017 / Accepted: 28 June 2017 / Published online: 19 July 2017

Abstract With increasing temperature, lipid bilayers undergo a gel-fluid phase transition, which plays an essential role in many physiological phenomena. In the present work, this first-order phase transition was investigated for variable heating and cooling rates for a dipalmitoylphosphatidylcholine (DPPC) lipid bilayer by means of atomistic molecular dynamics simulations. Alternative methods to track the melting temperature T_m are compared. The resulting T_m is shown to be independent of the scan rate for small heating rates (0.05–0.3 K/ns) implying reversible melting, and increases for larger heating (0.3–4 K/ns) or cooling rates (2–0.1 K/ns). The reported dependency of the melting temperature on the heating rate is in perfect agreement with a two-state kinetic rate model as suggested previously. Expansion and shrinkage, as well as the dynamics of melting seeds is described. The simulations further exhibit a relative shift between melting seeds in opposing membrane leaflets as predicted from continuum elastic theory.

Keywords Molecular dynamics · DPPC · Phase transition · Heating/cooling rate · Reversible melting · Melting seed

Electronic supplementary material The online version of this article (doi:10.1007/s00249-017-1237-3) contains supplementary material, which is available to authorized users.

✉ Rainer A. Böckmann
rainer.boeckmann@fau.de

[1] Computational Biology, Department of Biology, Friedrich-Alexander-University of Erlangen-Nürnberg, Staudtstrasse 5, Erlangen 91058, Germany

Introduction

Biological membranes form selectively permeable barriers within or around a cell, thereby allowing to establish and maintain specific biochemical environments. The predominant structural component of biological membranes is a lipid bilayer (Henn and Thompson 1969). Depending on the composition, temperature, pressure, or external fields, the bilayer structure may adopt various lamellar phases, namely crystalline (L_c), gel ($L_{\beta'}$), ripple ($P_{\beta'}$), and fluid (L_α, also referred to as liquid-crystalline) phases, given in the order of increasing temperature (Janiak et al. 1979). The first-order main phase transition from the gel to the fluid phase occurs at a critical melting temperature T_m during the heating process (Steim et al. 1969; Nagle 1980). This phase transition is characterized by the melting of the ordering of the hydrocarbon chains in the interior of the phospholipid bilayer (Chapman et al. 1966, 1967). The molecular structural changes are coupled to conformational changes of the lamellar membrane structure: during phase transition, the deformation of the alkyl chain *trans* configuration dominant in the gel phase to an increased level of *gauche*-orientations (Lippert and Peticolas 1972; Andreoli et al. 1980) induces the loss of the ordered lipid arrangement on a triangular lattice (Devaux and McConnell 1972; Tardieu et al. 1973), as well as a drastic increase in bilayer area (Traeubl and Sackmann 1972; Chapman 1975). Phase transitions of biomembranes are attracting increasing interest since this phenomenon may drastically affect essential cellular processes such as membrane permeabilization (Nagle and Scott 1978; Blicher et al. 2009), membrane fusion (Cevc and Richardsen 1999; Marrink and Peter Tieleman 2002), membrane poration (Leontiadou et al. 2004), membrane budding (Hurley et al. 2000), nerve pulse propagation (Heimburg and Jackson 2005;

Andersen et al. 2009), anesthesia (Trudell 1977), and cell lysis (Schmitt et al. 1993), and have been addressed in both atomistic (Qin et al. 2009; Schubert et al. 2011; Kowalik et al. 2015) and coarse-grained simulations on different scales (Marrink et al. 2005; Nagai et al. 2012; Kociurzynski et al. 2015; Hömberg and Müller 2010). Interestingly, since the transformation between distinct phases would likely as well alter the physiological functions that a lipid bilayer can carry out, bacteria change their lipid composition depending on the growth temperature such that the membrane keeps its optimal properties (Krasikova et al. 1995), remaining in the fluid phase also for the changed conditions.

The most commonly studied membrane, a dipalmitoylphosphatidylcholine (DPPC) lipid bilayer, undergoes the main phase transition at $T_m = 314.45$ K at an enthalpic cost of $\Delta H \approx 35$ kJ/mol (Mabrey and Sturtevant 1976; Biltonen and Lichtenberg 1993), determined using high-sensitivity differential scanning calorimetry (DSC) upon heating the lipid molecules in a multilamellar aqueous suspension at a scan rate of 0.1–0.5 K/min. Unfortunately, very few studies have been carried out tackling the dependency between the melting temperature and heating or cooling rates. For very high heating rates between 0.5 and 2 K/ns, atomistic molecular dynamics (MD) simulations predicted a logarithmic dependency of T_m on the heating rate (Schubert et al. 2011). Later on, this logarithmic dependency for large heating rates was interpreted within the framework of a two-state kinetic rate model (Kowalik et al. 2015), assuming a constant main transition temperature T_m for small rates. In this model, low rates r allow for reversible melting, while $T_m \propto log(r)$ is obtained for fast irreversible melting. However, reversible melting could not be observed in MD simulations yet at heating rates between 0.125 and 4 K/ns.

A "thermal hysteresis" with a broadened transition width was reported for DPPC multilamellar dispersions using deuterium magnetic resonance (DMR) investigations. For cooling from the fluid phase, T_m was ≈ 1 K lower as compared to heating of DPPC in the gel phase (Davis 1979). Later on, a reduction of the hysteresis change in T_m by 0.1–0.5 K between heating and cooling of DMPC liposomes for extremely slow temperature changes of 0.001 K/s using alternating current (AC) calorimetry was reported (Black and Dixon 1981). Additionally, the transition enthalpy ΔH was reduced to 40% during cooling as compared to heating. A similar phenomenon was seen in MD simulations of the phase transition of DSPC and DSPE lipid bilayers at a scan rate of 2 K/ns (Qin et al. 2009). It has been reported that this lack of convergence between transition pathways of heating and cooling processes is due to the occurrence of the metastable ripple or ripple-gel mixed phases (Tenchov 1991). Yet, detailed studies on the thermal hysteresis under different heating and cooling rates are still lacking.

Noteworthy, Kowalik et al. suggested that the chain-melting transition is initiated by a localized seed and followed by the propagation of its phase boundary (Kowalik et al. 2015). The critical role of a melting seed was as well suggested before, based on a kinetic model of nucleation theory (Kharakoz et al. 1993). In fact, such a seed initiation and its fast growth were observed both in the formation and the melting of a gel phase in coarse-grained simulations (Marrink et al. 2005). The authors described the membrane phase transition as a four-stage process: nucleation, growth, limited growth, and optimization. However, reported structural transitions based on MD simulations have been biased by the irreversible melting process during fast heating. The molecular mechanisms coupled to reversible melting during slow heating are still elusive.

The structural properties of a melting seed are likely comparable or coupled to the properties of membrane (nano) domain boundaries in general. In continuum elastic theory, the minimum perpendicular line tension along the rim between thick (gel) and thin (fluid) membrane domains could be achieved by shifting the rims between domains in opposing leaflets by a few nanometers relative to each other (Galimzyanov et al. 2015). Computational or experimental support for the arrangement of melting seeds in a gel bilayer, in particular at the domain boundaries, is still missing.

Here, atomistic molecular dynamics simulations were applied to study the membrane phase transition under variable heating and cooling rates. Alternative approaches for tracking the melting temperature T_m were systematically compared. The obtained dependency of T_m on the scan rate matches nicely with a two-state kinetic rate model (Kowalik et al. 2015). The thermal hysteresis for the phase transition between heating and cooling processes was addressed for different scan rates. The focus is put on reversible melting at low heating rates. Both the dynamics of melting seeds close to the main phase transition is characterized as well as the molecular arrangement of melting seeds within both membrane lipid leaflets.

Computational methods

Simulation systems

The lipid bilayer was composed of 288 tightly packed DPPC lipid molecules (144 lipids per leaflet), and solvated by 11,520 water molecules resulting in a lipid:water ratio of 1:40 (see Fig. 1) yielding a fully hydrated membrane (Tu et al. 1995; Feller et al. 1997). An initial configuration for

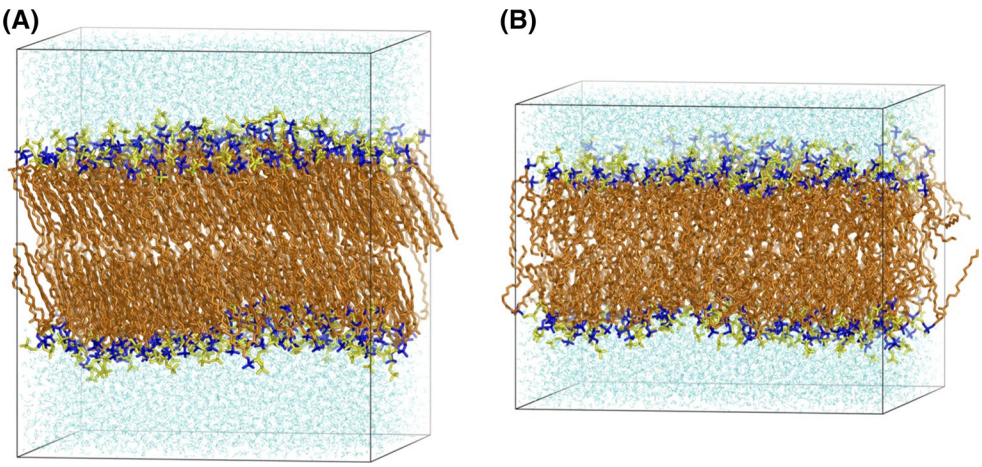

Fig. 1 3D view of the simulation box for a DPPC bilayer in the gel phase (**a**) and in the fluid (liquid crystalline) phase (**b**). Alkyl tails are shown as *orange sticks*, choline and phosphate groups in *yellow* and *blue*, respectively. Hydrogen atoms of the lipids are excluded for clarity. Water molecules are depicted as *thin lines in cyan*

the gel phase was obtained by initial equilibration of the bilayer at 320 K for 100 ns (Fig. 1a). This temperature is 5.5 K above the experimental melting temperature. Current force fields for lipids are not optimized for reproduction of membrane phase transitions. Already subtle changes may result in drastic shifts of T_m as shown for pentadecane (Siu et al. 2012). For improved statistics, six slightly different fully equilibrated configurations of the gel phase were chosen as starting structures and each heated at different scan rates (0.05, 0.1, 0.167, 0.3, 0.5, 1, 2, and 4 K/ns) to characterize the gel-fluid phase transition. Additionally, one gel-phase configuration was selected from a heating simulation (scan rate of 0.05 K/ns) and simulated for 400 ns to investigate the structural properties of melting seeds (temperature of 330.4 K, $\approx$ 4 K below T_m in MD). A template for the fluid structure was chosen at a temperature of 343 K and additionally equilibrated for 100 ns at fixed temperature (Fig. 1b). Six slightly different, fully equilibrated configurations of the fluid phase were chosen and each cooled at scan rates of 0.1, 0.167, 0.3, 0.5, 1, and 2K/ns in the study of the fluid-gel phase transition.

Simulation details

Atomistic molecular dynamics simulations were carried out with the open-source software GROMACS version 4.5.2 and the CHARMM36 force field for lipids (Brooks et al. 1983; Feller and MacKerell 2000; Hess et al. 2008). CHARMM36 yields a good area per lipid without applying any surface tension (Klauda et al. 2010). Also, other observables such as order parameters of both the lipid headgroup (DMPC) and of the acyl chains, the lipid self-diffusion coefficient, or the amino acid side chain insertion energies show good agreement to experiment (Pluhackova et al. 2016; Sandoval-Perez et al. 2017). A slightly modified form of the TIP3P water model (Jorgensen et al. 1983) used in CHARMM, known as TIPS3P model, was applied here for water parameters (MacKerell et al. 1998). Cut-off radii for van der Waals and Coulomb (short-range) potentials were both chosen to 1.2 nm (Klauda et al. 2010). Short-range electrostatic interactions were calculated explicitly, whereas long-range electrostatic interactions were computed using the particle mesh Ewald (PME) method (Darden et al. 1993). Temperature coupling was achieved with the v-rescale thermostat at a time constant of 0.1 ps (Bussi et al. 2007). The semi-isotropic pressure coupling was controlled using the Parrinello-Rahman algorithm with a time constant of 4.0 ps (Parrinello and Rahman 1981). The Lincs algorithm was used here in order to constrain the bond length of hydrogen atoms to a constant value (Hess et al. 1997). Periodic boundary conditions were applied in all three dimensions to avoid boundary effects caused by a finite simulation system. All subsequent analyses were performed using GROMACS analysis utilities, own scripts, and IDL programs (Fanning 2000). Molecular visualization was performed using the PyMOL program (Schrödinger 2015).

Calculation of the gauche density map

The lateral diffusion of phospholipids during heating is considerably slowed down as compared to diffusion in the fluid phase (data not shown). Therefore, melting seeds observed in the averaged gauche fraction are hardly subject to diffusion. Dihedral angles were analyzed for both *sn*1 and *sn*2 chains along the simulation time (every 500 ps). The averaged gauche fraction was analyzed for every lipid and its direct neighbors (clusters of typically seven lipids, i.e., a hexagonal lattice). For visualization, all lipids were assigned to a 10×10 grid for both layers. Each grid point was colored according to the averaged gauche fraction of the respective lipid clusters. Additionally, running averages were performed on three time frames. A

movie of the gel-fluid phase transition is provided in the Supplementary Information, visualizing the evolution of the melting seed during reversible melting.

Results and discussion

Gel and fluid phase DPPC structures

The membrane phase transition was studied in heating and cooling simulations at different rates ranging between 0.05 and 4 K/ns. For each heating and cooling rate, six simulations were carried out.

As a prerequisite step, the quality of the initial gel and fluid bilayer structures was addressed by analyzing the last 60-ns of 100-ns equilibrium simulations. The resulting areas per lipid were equilibrated with average values of 0.49 nm^2 for the gel phase and 0.63 nm^2 for the fluid phase. These values are in good agreement with the structural parameters determined from wide-angle X-ray scattering (WAXS) and nuclear magnetic resonance (NMR) spectroscopy experiments for fully hydrated DPPC bilayers, with (0.46 ± 0.02) nm^2 and (0.62 ± 0.02) nm^2, for the areas per lipid in the gel and fluid phase, respectively (Wiener et al. 1989; Nagle 1993). Another characteristic observable is the fraction of gauche bonds of the lipid tails. It is approximated here as the fraction of dihedral angles of each acyl chain in the range between −120° and 120°. As depicted in Fig. 2, a clear maximum is seen at the first dihedral position of the sn2 chain (red), in excellent agreement with experiment (Mendelsohn et al. 1989). The average fractions of gauche conformation are 0.15 and 0.32 for gel and fluid bilayers, respectively. Experimentally, approximate values of 0.1 (gel) and 0.3 (fluid) were reported for DPPC membranes (Davies et al. 1990; Picquart et al. 2003). Notably, both the area per lipid and the fraction of gauche dihedrals for the gel phase are increased as compared to experiment. This is partially due to local metastable distortions observed in the lower leaflet of the membrane (Fig. 1a), which is difficult to avoid in simulations (Schubert et al. 2011).

Tracking of the melting temperature

DPPC displays a first-order phase transition upon passage from the gel to fluid phase or reverse under heating or cooling, respectively (Biltonen and Lichtenberg 1993). During transition, the heat capacity c_p displays a sharp peak at the main phase transition temperature T_m. Accordingly, the enthalpy ΔH shows a step-like increase during transition, given by

$$\Delta H = \int_{T_1<T_m}^{T_2>T_m} c_p \mathrm{d}T. \tag{1}$$

Additionally, a number of structural observables like the area/lipid or the *trans-gauche* isomerization display pronounced changes upon phase transition. Different signatures for the passage between the gel and the fluid phase are compared in the following.

Change of enthalpy during phase transition

As displayed in Fig. 3a, the enthalpy grows approximately linearly both within the gel (g) and the fluid (l) phase with increasing temperature. At the phase transition temperature a sigmoidal jump in ΔH is observed. For the example displayed in Fig. 3 with a heating rate of 0.167 K/ns, T_m was determined to 333.4 K using the following sigmoidal fit function:

$$H = H^0 + c_p^g T + (\Delta H + \Delta c_p (T - T_m)) * \frac{1}{1 + \exp(-k(T - T_m))}. \tag{2}$$

H, c_p, T denote the system enthalpy, heat capacity, and temperature, respectively. ΔH corresponds to the total change in enthalpy for the $g \rightarrow l$ phase transition. Δc_p accounts for the difference between c_p in gel (c_p^g) and in fluid bilayers. k is the steepness of the enthalpy jump.

The heat capacity per lipid $c_{p.l}$ can be estimated by approximating the overall heat capacity by $c_p \cong c_{p.l} N_l + c_{p.w} N_w$, where N_l and N_w are the numbers of lipids (288) and water

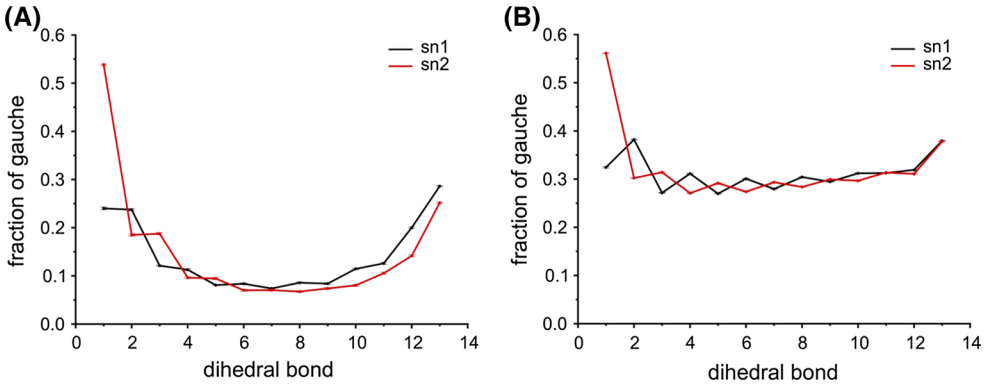

Fig. 2 Positional dependence of the gauche bond fraction of the *sn*1 (*black*) and *sn*2 (*red*) acyl tails in the gel phase (**a**) and in the fluid phase (**b**). The *plotted data* are average values of the last 60 ns of equilibrium MD simulations. The *error bars* were calculated using block averaging (six 10-ns blocks)

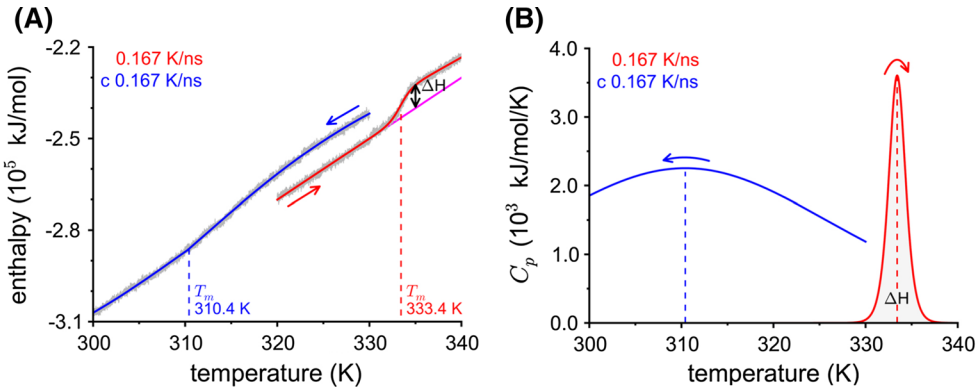

Fig. 3 **a** Tracking of the enthalpy as a function of temperature for both heating (*red*) and cooling (*blue*) at a rate of 0.167 K/ns. The *solid lines* show sigmoidal fits according to Eq. (2), yielding $T_m = 333.4$ K for heating and $T_m = 310.4$ K for cooling. The *magenta line* is the baseline. **b** Evolution of the excess heat capacity $c_{p.x}$ as a function of temperature during phase transition. The *grey area* below the $c_{p.x}$ curve is the change in enthalpy during phase transition, ΔH. The *arrows* depict the direction of the temperature increments

molecules (11,520), respectively. $c_{p.w}$ is the water heat capacity. The TIPS3P water model applied here has similar physical properties to TIP3P (Jorgensen et al. 1983; MacKerell et al. 1998), with $c_{p.w} = 0.079$ kJ/mol/K for bulk water (Vega and Abascal 2011). This value is in good agreement with the experimental value of 0.075 kJ/mol/K (Ginnings and Furukawa 1953). With these settings, $c_{p.l} \approx 3.8$ kJ/mol/K and $c_{p.l} \approx 2.7$ kJ/mol/K are obtained for gel and fluid bilayers, respectively. Note that this value is considerably larger than the experimental value for the lipid heat capacity of 1.6 kJ/mol/K for the gel phase, and of 1.7 kJ/mol/K for the fluid phase (Blume 1983).

In turn, a reduced lipid heat capacity of $c_{p.l} \approx 0.9$ kJ/mol/K was reported from MD simulations using a united atom model for DPPC (Kowalik et al. 2015). Together, these data suggest that the all-atom membrane model employed here reflects a relatively higher degree of freedom as compared to experiment. However, additional effects on the lipid heat capacity arising, e.g., from the finite membrane patch size or the level of hydration (Marrink et al. 2005) cannot be excluded.

In addition, the excess heat capacity ($c_{p.x}$) was calculated by the derivative of the enthalpy against the temperature (Eq. 2), followed by a baseline subtraction where both c_p and Δc_p were removed. As elucidated in Fig. 3b, a distinct peak can be identified at the critical melting point for the excess heat capacity ($c_{p.x}$) curve. The transition enthalpy and entropy are obtained from:

$$\Delta H = \int_{T_0}^{T_1} c_{p.x} \mathrm{d}T, \quad \text{and} \tag{3}$$

$$\Delta S = \int_{T_0}^{T_1} \frac{c_{p.x}}{T} \mathrm{d}T. \tag{4}$$

T_0 and T_1 were chosen as the lower and upper limits of the temperature range in the heating and cooling simulations.

The changes in enthalpy and entropy per lipid for the gel-fluid DPPC phase transition were determined to $\Delta h = (30.9 \pm 0.7)$ kJ/mol and $\Delta s = (92.4 \pm 2.2)$ J/mol/K. These observables were calculated according to Eqs. (1) and (4), normalized by the number of lipids and averaged over all heating simulations at the rate of 0.05, 0.1, 0.167, and 0.3 K/ns. Note that these values are slightly below the experimental $\Delta h = 35$ kJ/mol (Mabrey and Sturtevant 1976; Biltonen and Lichtenberg 1993), and $\Delta s = (119 \pm 1)$ J/mol/K determined from MD simulations (Kowalik et al. 2015). In contrast to heating, the enthalpy change during cooling scans does not display a clear signature of phase transition (Fig. 3).

Membrane structural changes during phase transition

A structural measure for membrane phase transitions is the area per lipid. As shown in Fig. 4a, a distinct jump is seen during phase transition in the heating simulations (rate of 0.167 K/ns in Fig. 4) between ≈0.50 nm^2 (gel phase) and ≈0.63 nm^2 (liquid-crystalline phase). Differently, the reverse transition during cooling is broadened and significantly shifted to a lower melting temperature T_m. T_m was determined to 333.8 K for heating (red curve) and 317.4 K for cooling (blue curve) at a heating/cooling rate of 0.167 K/ns. The melting temperature determined from the area per lipid during heating is 0.4 K above the one calculated from the corresponding curve shape of the enthalpy (Fig. 3),

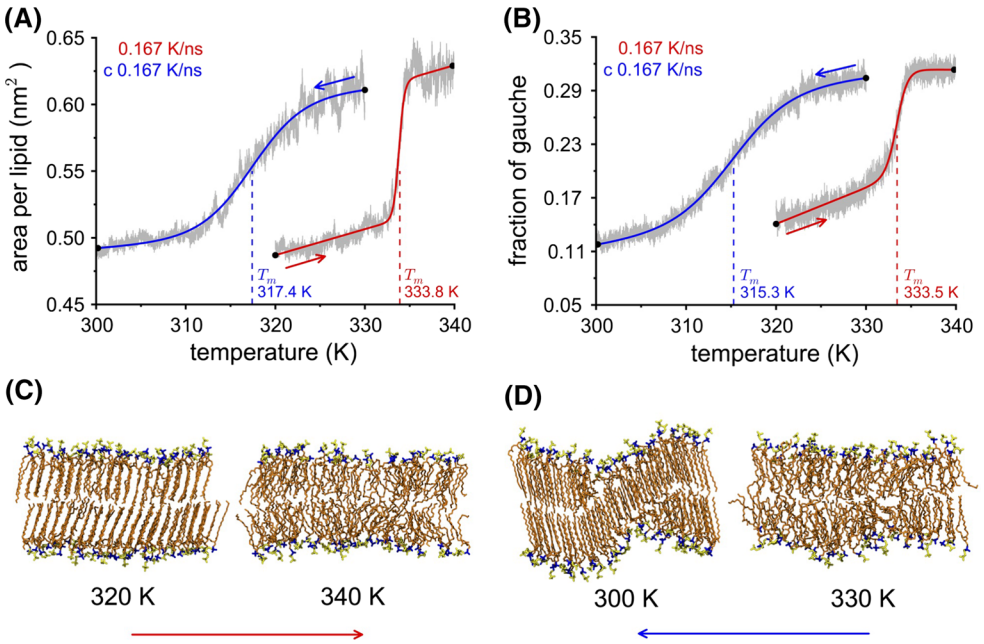

Fig. 4 Tracking of the area per lipid (**a**) and the fraction of gauche dihedrals (**b**) in the determination of T_m, at a scan rate of 0.167 K/ns. The *red* and *blue solid lines* show sigmoidal fits for the heating and cooling processes, respectively. Representative snapshots of bilayer structures (*black dots* in melting curves at the first and last time frames) are displayed for heating (**c**) and cooling (**d**) simulations. Lipid tails are shown as *orange*, choline groups as *yellow* and phosphate groups as *blue sticks*. Hydrogen atoms are excluded for clarity. The *red* and *blue arrows* depict the direction of temperature increments

indicating a delay in the evolution of the area per lipid during the melting process. The end states between heating and cooling simulations differ significantly: While a one-step transition between gel and fluid phase is observed during heating, the reverse process got trapped in an intermediate ripple-like phase (see Fig. 4c, d). Experimentally, this ripple phase was observed in a low enthalpy pre-transition below T_m during heating (Janiak et al. 1976; Heimburg 2000; Riske et al. 2009). Note that different intermediate structures in ripple-gel mixed phases were formed during different cooling scans (not shown here).

A second structural measure for phase transitions is given by the fraction of acyl chain gauche dihedrals. As shown in Fig. 4b, the acyl chains of the DPPC membrane largely adopt a *trans* configuration in the gel phase. During melting, the bilayer structure undergoes a rapid *trans* to gauche rotational isomerization. T_m was determined from a sigmoidal fit to the dihedral transition to 333.5 and 315.3 K for the heating and cooling processes at 0.167 K/ns, respectively. Note that the resulting T_m for different heating rates are in good agreement with those obtained by enthalpy fitting (see above). The comparatively large jumps both for heating and for cooling and the significantly enhanced statistics as compared to the area per lipid render this observable particularly suitable in the determination of the melting temperature during membrane phase transition.

Figure 5 shows the evolution of the fraction of gauche dihedrals as a function of temperature for six replica simulations of each setup for both heating (red lines) and cooling (blue) simulations at two scan rates of 0.167 and 0.2 K/ns, respectively. The transition from gel to fluid phases was analyzed to (334.1 ± 0.5) K for heating and (316.1 ± 0.6) K for cooling processes at a scan rate of 0.167 K/ns, and to (343.1 ± 0.2) K for heating and (306.2 ± 1.4) K during cooling at a scan rate of 2 K/ns. i.e., a significant hysteresis was observed during cooling process as compared to heating. Additionally, the transition width is significantly broadened during cooling (Fig. 5). These findings agree well with experimental studies mentioned above (Davis 1979; Black and Dixon 1981). The steepness of the jumps decreased with increasing velocity both for heating and for cooling. The fastest scan rate of 2 K/ns led to a quasi-continuous phase transition. Data for T_m as determined from simulations for different heating and cooling rates are collected in Table 1.

Dependency of T_m on heating/cooling rates

As observed previously, the apparent melting temperature depends on the rate of heating or cooling (Schubert et al. 2011; Kowalik et al. 2015). The transition temperatures depend for both heating and cooling simulations linearly on the logarithm of the rate of temperature change at scan rates above 0.3 K/ns, displaying a similar slope. Such a symmetry has been shown via differential scanning calorimeters (DSC) for various materials that undergo a first-order phase transition (Neuenfeld and Schick 2006). Empirically, a similar dependency of T_m on the rate of temperature change can be predicted assuming a first-order phase transition for scan rates well above the membrane relaxation time.

The linear increase of T_m with $\ln(r)$ changes abruptly for heating rates below $r^{eq} \leq 0.3$ K/ns with an approximately

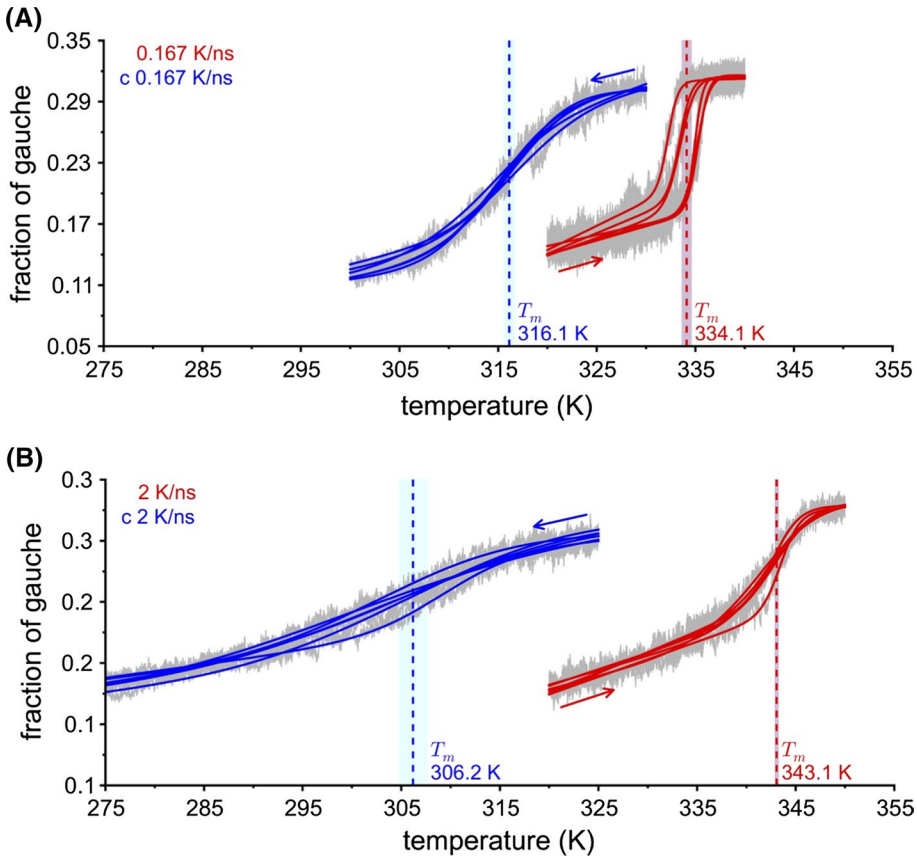

Fig. 5 Fraction of acyl chain gauche dihedrals as a function of temperature for the scan rates of 0.167 K/ns (**a**) and 2 K/ns (**b**). The *red* and *blue solid lines* show sigmoidal fits for the heating and cooling processes, used to determine the transition temperature T_m to 334.1 and 316.1 K (**a**), and 343.1 and 306.2 K (**b**), respectively. The *dashed lines* mark T_m obtained from averaging over six replica simulations, and the *shaded areas* mark the standard deviations. The *red* and *blue arrows* depict the direction of the temperature increments

Table 1 Phase transition temperatures and hysteresis of the DPPC lipid bilayer under variable heating and cooling rates, calculated by tracking the fraction of gauche dihedrals during phase transition

r (K/ns)	T_m – heating (K)	T_m – cooling (K)	Hysteresis (K)
0.05	334.5 ± 0.9	–	–
0.1	332.8 ± 0.7	317.5 ± 0.6	15.3 ± 0.9
0.167	334.1 ± 0.5	316.1 ± 0.6	18.0 ± 0.8
0.3	334.5 ± 0.8	314.4 ± 0.7	20.1 ± 1.1
0.5	337.6 ± 0.8	312.4 ± 0.6	25.2 ± 1.0
1	339.5 ± 0.4	309.3 ± 1.1	30.2 ± 1.2
2	343.1 ± 0.2	306.2 ± 1.4	36.9 ± 1.4
4	348.1 ± 0.7	–	–

constant transition temperature of 333.8 ± 0.4 K. The T_m dependency for faster temperature changes shows a symmetric behavior for the heating and cooling processes. This scan rate dependency of T_m is in perfect agreement with a two-state kinetic rate model proposed by Kowalik et al. (2015), which will be discussed in more detail in the next section.

It is important to note that T_m in heating is always larger than for cooling with a difference of approx. 19 K even for low scan rates (≤0.3 K/ns) (see Fig. 6). As a matter of fact, it has been demonstrated that these two thermodynamic events follow different phase transition pathways due to the occurrence of the metastable ripple or ripple-gel mixed phases (Tenchov 1991). This is also supported by the observation of two-phase coexistence, which is thermodynamically allowed in two-component systems such as lipids in water (Callen 1960). In fact, it has been established that both ordered and disordered structures simultaneously exist in a lipid bilayer upon cooling in the fluid phase (Leekumjorn and Sum 2007). For the formation of an unperturbed gel structure, isothermal annealing out of the transition region is required (Tsuchida et al. 1987). As shown in Fig. 7, the thermal hysteresis for heating/cooling simulations increases with increasing scan rates (≥0.3 K/ns). A linear relationship is obtained between the hysteresis and the logarithm of the scan rates (for $r \geq 0.3$ K/ns).

Two-state kinetic rate model

The heating rate dependency of T_m discussed above supports a recently suggested two-state kinetic rate model (Kowalik et al. 2015): following this model, the membrane phase transition can be described by (i) a slow-heating reversible melting, close to thermal equilibrium, where the transformation

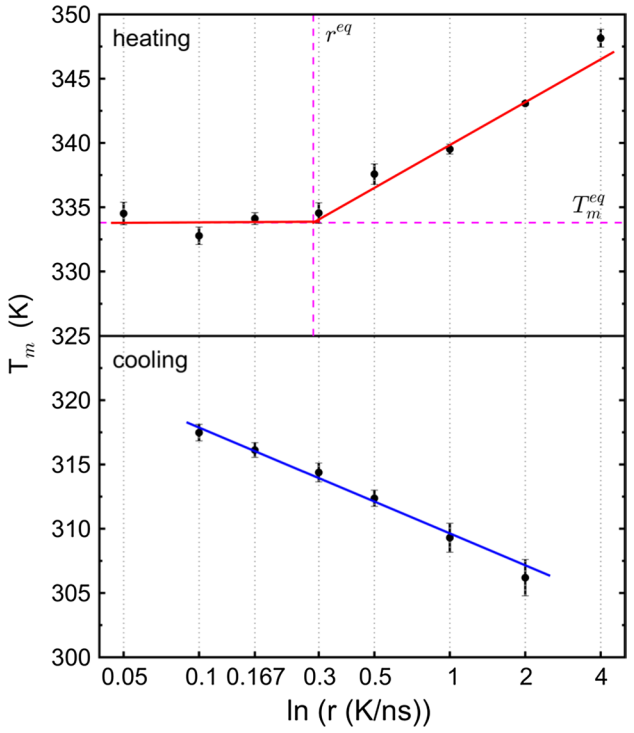

Fig. 6 Dependency of T_m on the natural logarithm of the scan rate r both for heating and cooling processes. The *error bars* represent the standard deviations of the mean determined from six simulations for each scan rate. The *red* and *blue curves* denote linear fits of phase transition temperatures for heating and cooling processes, respectively

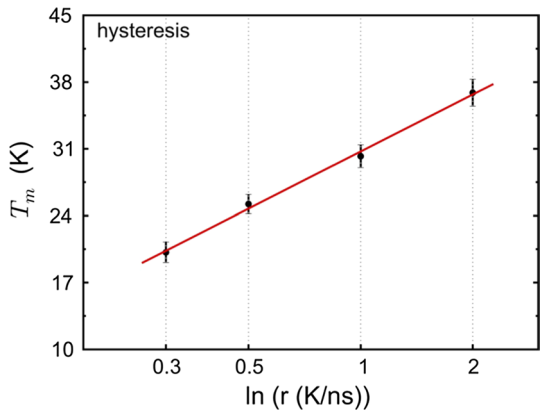

Fig. 7 Linear dependency of the thermal hysteresis for the gel-fluid phase transition temperature under heating and cooling on the logarithm of the scan rate r (*red solid line*). The *error bars* represent standard deviations

between gel and fluid phases occurs in both directions, and (ii) a fast-heating unidirectional melting at non-equilibrium. Based on this differentiation, a critical equilibrium heating rate r_{eq} is introduced that separates slow- and fast-heating regimes. For the fast-heating regime, irreversible melting can be assumed. Then, the heating rate dependency of the apparent melting temperature T_m close to r_{eq} can be approximated by Kowalik et al. (2015):

$$T_m(r) \approx T_m^{\mathrm{eq}} + \frac{T_m^{\mathrm{eq}2}}{\theta} \ln\left(\frac{r}{r_{\mathrm{eq}}}\right), \tag{5}$$

with the equilibrium melting temperature T_m^{eq}, and a scaling parameter θ given by:

$$\Delta H_{gl}^* = R\theta. \tag{6}$$

ΔH_{gl}^* is the activation enthalpy for the gel-fluid phase transition, and R represents the gas constant (8.3145 J/K/mol).

The equilibrium transition temperature was determined to $T_m^{\mathrm{eq}} = (333.8 \pm 0.4)$ K by averaging T_m in the slow-heating regime ($r = 0.05 - 0.167$ K/ns) with $r^{\mathrm{eq}} = (0.285 \pm 0.035)$ K/ns (Eq. 5). The activation enthalpy for the gel-fluid phase transition is given by (192.6 ± 11.8) kJ/mol.

More generally, the activation enthalpy can additionally be assessed using the Kissinger method (Kissinger 1957) for the solution of the irreversible melting in the two-state model (see Kowalik et al. 2015 for details). Here, the change in T_m for different fast-heating or cooling rates (fast-scan irreversible phase transitions) allows an estimate for the respective activation enthalpies without knowledge about the equilibrium rate constant:

$$\ln\left(\frac{r}{T_m^2}\right) = \ln\left(\frac{ZR}{\Delta H^*}\right) - \frac{\Delta H^*}{RT_m}. \tag{7}$$

r is the scan rate, Z is a pre-exponential factor.

As shown in Fig. 8, a linear fit between $\ln(r/T_m^2)$ and $1/T_m$ based on Eq. (7) is applied both for heating (A) and for cooling (B) processes. The activation enthalpies for the gel-fluid and fluid-gel phase transitions of the DPPC lipid bilayer were determined to $\Delta H_{gl}^* = (193.9 \pm 11.9)$ kJ/mol and $\Delta H_{lg}^* = (-234.2 \pm 24.3)$ kJ/mol, respectively.

Reversible melting

Special attention is given in the following to the slow-heating reversible melting regime as this could not be described before based on MD simulations. Chain melting is initiated by a localized seed and followed by its propagation (Marrink et al. 2005; Kowalik et al. 2015). According to the two-state kinetic rate theory, transitions between gel $L_{\beta'}$ and fluid L_α phases during reversible melting should occur in both directions. Here, we analyzed the existence of melting seeds, their size, shape, and positional fluctuations close to phase transition.

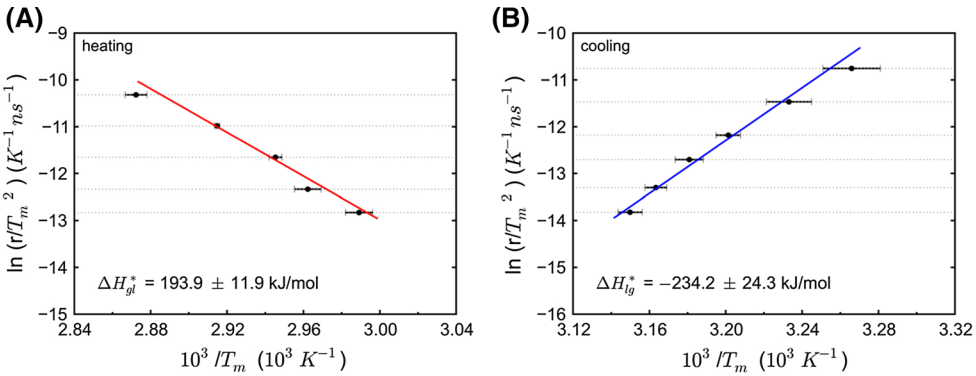

Fig. 8 Linear fit between $\ln(r/T_m^2)$ and $10^3/T_m$ used in the analysis of the activation enthalpy ΔH^* on the basis of the Kissinger's equation (Eq. 7). The *red* (**a**) and *blue* (**b**) curves indicate the fitting for heating (0.3–4 K/ns) and cooling (2–0.1 K/ns) processes. Standard deviations are given as *error bars*

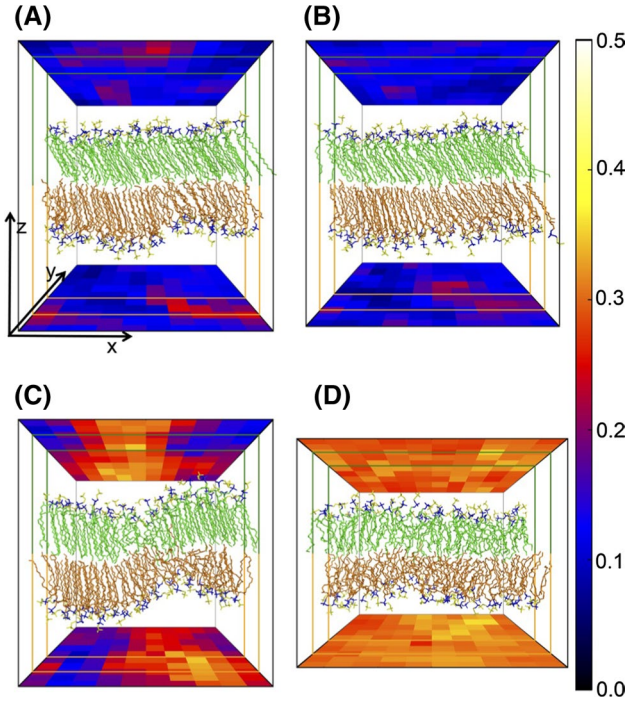

Fig. 9 Density maps of gauche fractions in individual lipid layers for four snapshots (0.5, 26, 288, and 399.5 ns) below (**a**, **b**), at (**c**), and above (**d**) the phase transition temperature for a heating simulation at a rate of 0.05 K/ns. The corresponding structures are shown as well. Alkyl tails are *colored green* (*upper layer*) and *orange* (*lower layer*), choline and phosphate groups are *colored yellow* and *blue*, respectively. Hydrogen atoms from the lipids are excluded for clarity. The *color bar* is defined by the percentage of gauche rotamers

Direct demonstration of reversible melting

Density maps of gauche fractions of lipid tails were recorded as a direct representation of melting seeds for slow heating simulations ($r = 0.05$ K/ns). As a prerequisite step, the expected average size of a seed (n_l, number of lipids) was determined from the activation energy and transition enthalpy (Δh, per lipid) on the basis of the two-state kinetic rate model $n_l = \Delta H^*/\Delta h$, yielding an expected seed size of 6.2 ± 0.4 lipids. This is consistent with the proposed minimum seed size of 7 as determined from calorimetric measurements (Kharakoz and Shlyapnikova 2000) and previous MD simulations using the united-atom Berger lipid force field (Kowalik et al. 2015).

The evolution of the melting of a phospholipid bilayer is shown for four sample snapshots in Fig. 9 below (a, b), at (c), and above the phase transition temperature (d). Apart from the structure, density maps of the gauche fraction of the lipid tails for both monolayers are displayed as well. The fraction of gauche mainly ranges from 0.15 (gel phase, colored blue) to 0.32 (fluid phase, orange). The initial bilayer structure (a) reveals a few distortions of the gel structure which, however, vanish or shrink considerably during the first nanoseconds (b) (see also Fig. 10 below). Thus, the initial ordering in the simulation system does not bias the location of melting seeds for reversible melting. Close to melting transition (c), "ripples" can be identified, indicative of a membrane ripple phase. This co-existence of gel and fluid domains has been reported from neutron diffraction during the main phase transition (Armstrong et al. 2012). Finally, most lipids exhibit a gauche configuration in the fluid phase (d).

The appearance, disappearance, and mobility of lipid melting seeds are displayed for different temperatures and separately for each lipid monolayer in Fig. 10c. The evolution of the fraction of gauche dihedrals is highly correlated between the two monolayers (Fig. 10b) and displays accordingly the same phase transition temperature, i.e., the lipid monolayers are tightly coupled (see also Kowalik et al. 2015). The melting seeds expand and shrink during the simulation in both monolayers. Additionally, positional fluctuations of the melting seeds in the individual layers are clearly seen in Fig. 10c. These size fluctuations, as well as displacements of the melting seed due to the occurrence of transitions between gel and fluid phases in both directions hint to fully reversible melting transition at the studied heating rate of 0.05 K/ns.

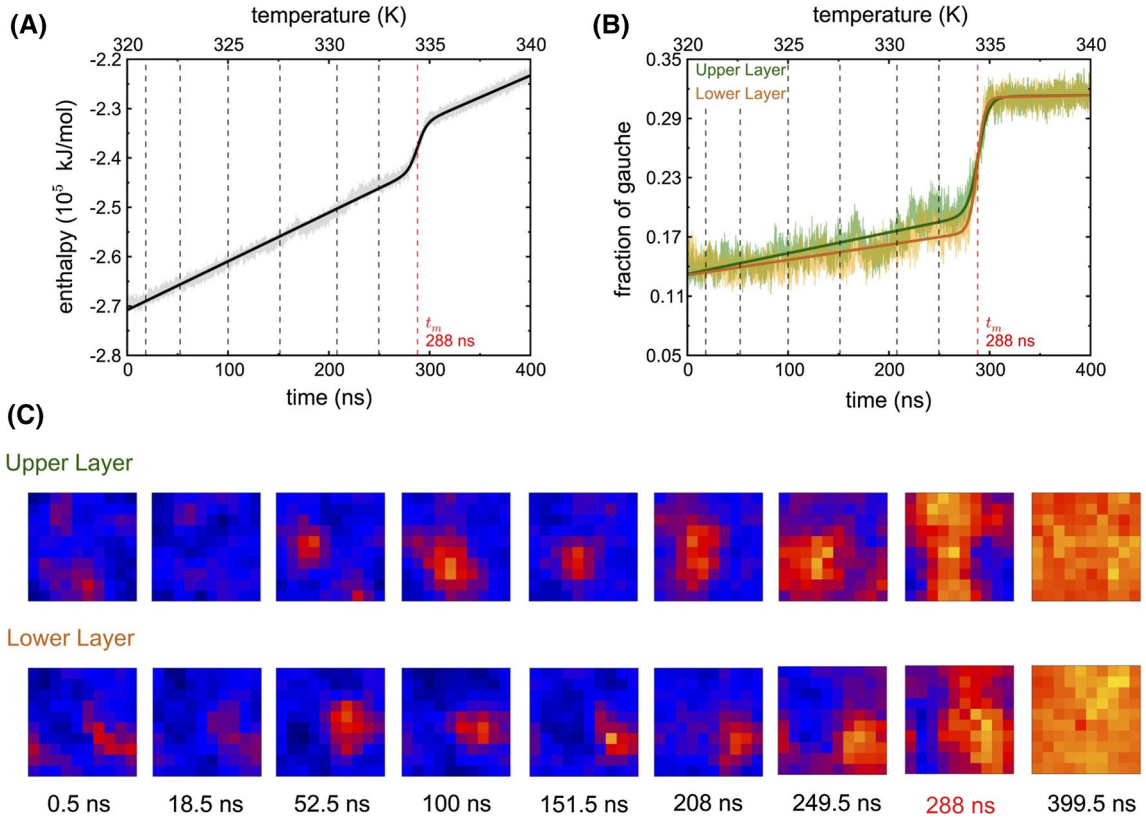

Fig. 10 Tracking of the enthalpy (**a**) and the fraction of gauche dihedrals for both lipid monolayers (**b**) as a function of temperature and simulation time. The *vertical dashed lines* indicate intermediate structures whose density maps of gauche fractions are shown in **c**. The melting temperature (reached at $t_m = 288$ ns) is highlighted by *red dashed lines*

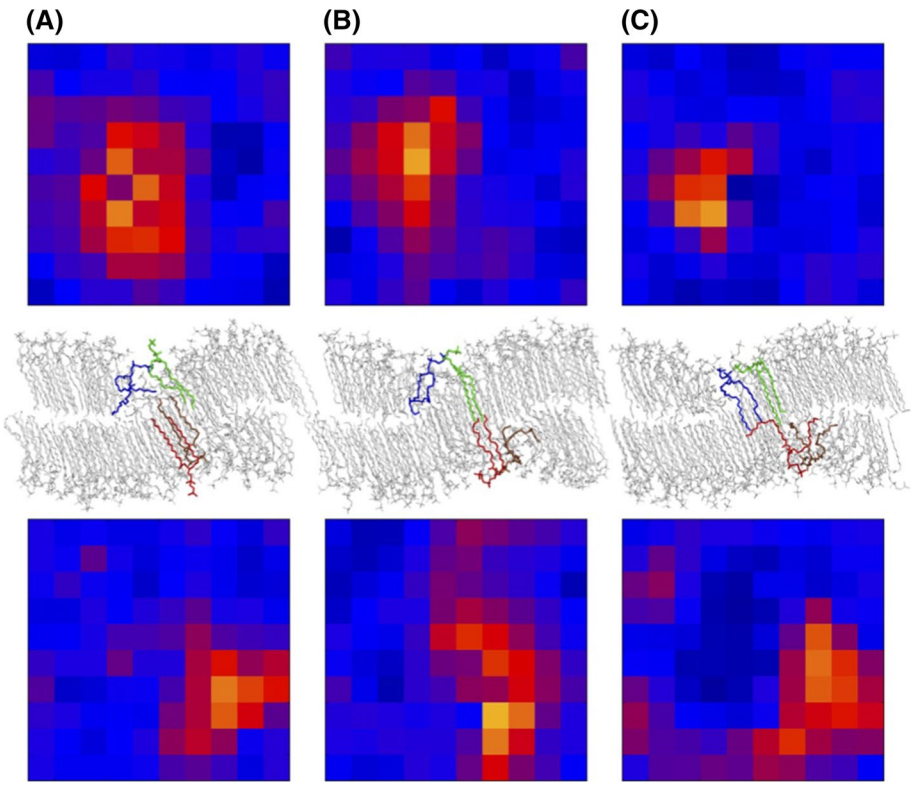

Fig. 11 Densities of gauche fraction for both lipid layers at three different time frames (0.5, 195.5, and 399.5 ns) from an equilibrium MD simulation slightly below the phase transition temperature at $T = 330.4$ K. Lipid molecules are shown as *grey sticks*. Four lipids are highlighted in *blue*, *green*, *red*, and *brown* in order to describe their specific configurations at different times. Hydrogen atoms are excluded for clarity

Characterization of the melting seed

In order to further characterize positional changes of the melting seeds in the individual monolayers, we performed a 400-ns equilibrium simulation at a constant temperature of $T = 330.4$ K (4 K below T_m) (see movie in Supplementary Information). Snapshots separated by roughly 200 ns (0.5 ns (a), 195.5 ns (b), 399.5 ns (c)) are displayed in Fig. 11. Firstly, the formation of partially interdigitated structures for the melting seeds is observed resembling 'ripple' formation. The melting seed propagates during the simulation to the left, as is seen in the gauche density maps, and as well in the displayed bilayer configurations: e.g., two lipids (colored blue and green) at the right edge of the melting seed in the upper layer (Fig. 11) change from a disordered to an ordered configuration, and two initially ordered lipids (red and brown) at the left edge of the melting seed in the lower layer pass over to a disordered configuration.

The melting seeds in the individual lipid layer have a size of 1.5–2 nm (Fig. 12a). Interestingly, the melting seeds in the opposing monolayers are laterally shifted by (3.8 ± 0.4) nm (Fig. 12b) This value is in astonishingly good agreement with a recent prediction of 4 nm for the optimal shift of the rims of opposing leaflets between ordered and disordered domains based on continuum elastic theory (Galimzyanov et al. 2015).

Conclusions

The physical properties of the phospholipid bilayer thermal phase transition for variable heating and cooling rates was addressed, based on a series of atomistic molecular dynamics simulations of a fully hydrated DPPC lipid bilayer. A systematic comparison of different approaches to determine the melting temperature prompted to the fraction of acyl chain gauche dihedrals showing the most immediate and distinct change upon phase transition. The simulations showed a "thermal hysteresis" with a broadened transition width for cooling as compared to heating. Also, the phase transition during cooling did not follow the same configurational pathway as during heating, and resulted in distinct metastable phases (ripple phase or gel-ripple mixed phase) instead of a well-defined gel structure.

The dependency of the melting temperature on the scan rate was determined for both heating and cooling. T_m remained approximately unchanged for low heating rates (0.05–0.3 K/ns), and increased linearly with the logarithm of the rate of temperature change for larger heating (0.3–4 K/ns) and cooling rates (2–0.1 K/ns). These results are in perfect agreement with a two-state kinetic rate model (Kowalik et al. 2015). Furthermore, the change in T_m with the scan rate ($\geq$0.3 K/ns) is symmetric for heating and cooling.

Based on the two-state kinetic rate model, several thermodynamic parameters were determined for the DPPC gel-fluid phase transition. The equilibrium melting temperature was calculated to $T_m^{eq} = (333.8 \pm 0.4)$ K, which is approx. 19 K above the experimental value. However, different force fields were shown to yield significantly different results for the main phase transition temperature (Pluhackova et al. 2016), displaying a huge sensitivity towards small changes in force field parameters (Siu et al. 2012). Future force field improvements for lipids (Pluhackova et al. 2016) and mixed protein-lipid systems (Sandoval-Perez et al. 2017) will therefore likely put an additional focus on the proper description of phase transitions as done already for hydrocarbon chains (Siu et al. 2012). In turn, the overall phase transition behavior is likely less affected by the choice of the particular force field. E.g., the transition steepness or transition width for DPPC were shown to be similar for the CHARMM36 (Klauda et al. 2010) and both the Lipid14 (Dickson et al. 2014) and Slipids (Jämbeck and Lyubartsev 2012) force fields (Pluhackova et al. 2016). Here, the critical equilibrium heating rate for DPPC within the

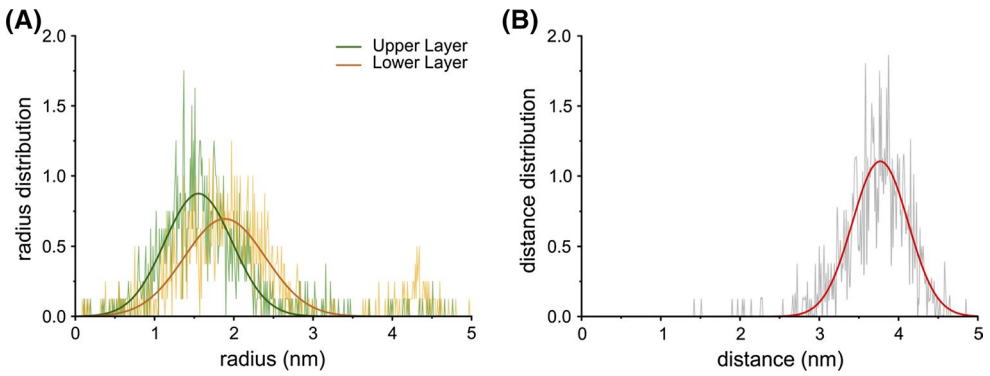

Fig. 12 **a** Gaussian distribution of the seed radius in *upper* (*green*) and *lower* (*orange*) lipid layers. The radius was determined to include the clustered lipids with an average gauche dihedral contribution >0.235. **b** Gaussian distribution of the lateral distance between the centers of melting seeds in opposite monolayers (*red*), defined by the lipids with an average gauche dihedral contribution >0.235

CHARMM force field was determined to $r^{eq} = (0.285 \pm 0.035)$ K/ns. It separates reversible from irreversible processes during melting. The activation enthalpy for phase transition is $\Delta H^*_{gl} = (192.6 \pm 11.8)$ kJ/mol, suggesting melting seed sizes of 6–7 lipids.

Reversible melting simulations displayed both expansion and shrinkage as well as displacements of melting seeds (see phase transition movie, Supplementary Information). Pre-applied localized melting seeds in the initial gel structure did not alter the transition for reversible melting. Additionally, a shift in relative positions of melting seeds between the opposing lipid leaflets was identified, in excellent agreement with recent theoretical considerations based on continuum elastic theory (Galimzyanov et al. 2015). A partially interdigitated 'ripple' structure was observed between the melting seed and its neighboring lipids, which likely reduces the line tension (Debnath et al. 2014; de Vries 2005).

For the first time, reversible phase transitions could be observed in atomistic MD simulations of lipid bilayers, yielding a conclusive view on the thermodynamics of heating and cooling, as well as on the structure and dynamics of melting seeds, i.e., on the formation of nanodomains in single-component membranes. Similarly, membrane MD simulations (Pluhackova and Böckmann 2015) will be a valuable tool in the characterization of domain formation also in multicomponent biomembrane mimetics close to phase transition, and the influence of these domains, e.g., on the distribution of proteins and lipids.

Acknowledgements This work was supported by the German Science Foundation (DFG) within the Research Training Group 1962—Dynamic Interactions at Biological Membranes, the SFB1027—Physical Modeling of Non-Equilibrium Processes in Biological Systems, and by a scholarship from the China Scholarship Council (CSC, to LS).

References

Andersen SS, Jackson AD, Heimburg T (2009) Towards a thermodynamic theory of nerve pulse propagation. Prog Neurobiol 88(2):104–113

Andreoli TE, Hoffman JF, Fanestil DD, Schultz SG (1980) Membrane physiology. Springer, Berlin

Armstrong CL, Barrett M, Toppozini L, Kučerka N, Yamani Z, Katsaras J, Fragneto G, Rheinstädter MC (2012) Co-existence of gel and fluid lipid domains in single-component phospholipid membranes. Soft Matter 8(17):4687–4694

Biltonen RL, Lichtenberg D (1993) The use of differential scanning calorimetry as a tool to characterize liposome preparations. Chem Phys Lipids 64(1):129–142

Black S, Dixon G (1981) Alternating current calorimetry of dimyristoylphosphatidylcholine multilayers: hysteresis and annealing near the gel to liquid-crystal transition. Biochemistry 20(23):6740–6744

Blicher A, Wodzinska K, Fidorra M, Winterhalter M, Heimburg T (2009) The temperature dependence of lipid membrane permeability, its quantized nature, and the influence of anesthetics. Biophys J 96(11):4581–4591

Blume A (1983) Apparent molar heat capacities of phospholipids in aqueous dispersion. Effects of chain length and head group structure. Biochemistry 22(23):5436–5442

Brooks BR, Bruccoleri RE, Olafson BD, Swaminathan S, Karplus M et al (1983) Charmm: a program for macromolecular energy, minimization, and dynamics calculations. J Comput Chem 4(2):187–217

Bussi G, Donadio D, Parrinello M (2007) Canonical sampling through velocity rescaling. J Chem Phys 126(1):014,101

Callen H (1960) Thermodynamics: an introduction to the physical theories of equilibrium thermostatics and irreversible thermodynamics. Wiley, New York

Cevc G, Richardsen H (1999) Lipid vesicles and membrane fusion. Adv Drug Deliv Rev 38(3):207–232

Chapman D (1975) Phase transitions and fluidity characteristics of lipids and cell membranes. Q Rev Biophys 8(02):185–235

Chapman D, Byrne P, Shipley G (1966) The physical properties of phospholipids. I. Solid state and mesomorphic properties of some 2, 3-diacyl-dl-phosphatidylethanolamines. Proc R Soc Lond Ser A 290(1420):115–142

Chapman D, Williams R, Ladbrooke B (1967) Physical studies of phospholipids. VI. Thermotropic and lyotropic mesomorphism of some 1, 2-diacyl-phosphatidylcholines (lecithins). Chem Phys Lipids 1(5):445–475

Darden T, York D, Pedersen L (1993) Particle mesh Ewald: an N· log (N) method for Ewald sums in large systems. J Chem Phys 98(10):089

Davies MA, Brauner JW, Schuster HF, Mendelsohn R (1990) A quantitative infrared determination of acyl chain conformation in gramicidin/dipalmitoylphosphatidylcholine mixtures. Biochem Biophys Res Commun 168(1):85–90

Davis JH (1979) Deuterium magnetic resonance study of the gel and liquid crystalline phases of dipalmitoyl phosphatidylcholine. Biophys J 27(3):339

Debnath A, Thakkar FM, Maiti PK, Kumaran V, Ayappa K (2014) Laterally structured ripple and square phases with one and two dimensional thickness modulations in a model bilayer system. Soft Matter 10(38):7630–7637

Devaux P, McConnell H (1972) Lateral diffusion in spin-labeled phosphatidylcholine multilayers. J Am Chem Soc 94(13):4475–4481

de Vries AH, Yefimov S, Mark AE, Marrink SJ (2005) Molecular structure of the lecithin ripple phase. Proc Natl Acad Sci USA 102(15):5392–5396

Dickson CJ, Madej BD, Skjevik AA, Betz RM, Teigen K, Gould IR, Walker RC (2014) Lipid14: the Amber lipid force field. J Chem Theory Comput 10(2):865–879

Fanning DW (2000) IDL programming techniques. Fanning software consulting, Fort Collins

Feller SE, MacKerell AD (2000) An improved empirical potential energy function for molecular simulations of phospholipids. J Phys Chem B 104(31):7510–7515

Feller SE, Venable RM, Pastor RW (1997) Computer simulation of a DPPC phospholipid bilayer: structural changes as a function of molecular surface area. Langmuir 13(24):6555–6561

Galimzyanov TR, Molotkovsky RJ, Bozdaganyan ME, Cohen FS, Pohl P, Akimov SA (2012) Elastic membrane deformations govern interleaflet coupling of lipid-ordered domains. Phys Rev Lett 115(8):088,101

Ginnings D, Furukawa G (1953) Heat capacity standards for the range 14–1200 degrees K.-correction. J Am Chem Soc 75(24):6359–6359

Heimburg T (2000) A model for the lipid pretransition: coupling of ripple formation with the chain-melting transition. Biophys J 78(3):1154–1165

Heimburg T, Jackson AD (2005) On soliton propagation in biomembranes and nerves. Proc Natl Acad Sci USA 102(28):9790–9795
Henn FA, Thompson TE (1969) Synthetic lipid bilayer membranes. Annu Rev Biochem 38(1):241–262
Hess B, Bekker H, Berendsen HJ, Fraaije JG et al (1997) Lincs: a linear constraint solver for molecular simulations. J Comput Chem 18(12):1463–1472
Hess B, Kutzner C, Van Der Spoel D, Lindahl E (2008) GROMACS 4: algorithms for highly efficient, load-balanced, and scalable molecular simulation. J Chem Theory Comput 4(3):435–447
Hurley JH, Boura E, Carlson LA, Różycki B (2010) Membrane budding. Cell 143(6):875–887
Hömberg M, Müller M (2010) Main phase transition in lipid bilayers: phase coexistence and line tension in a soft, solvent-free, coarse-grained model. J Chem Phys 132(155):104
Janiak MJ, Small DM, Shipley GG (1976) Nature of the thermal pretransition of synthetic phospholipids: dimyristoyl- and dipalmitoyllecithin. Biochemistry 15(21):4575–4580
Janiak MJ, Small DM, Shipley GG (1979) Temperature and compositional dependence of the structure of hydrated dimyristoyl lecithin. J Biol Chem 254(13):6068–6078
Jorgensen WL, Chandrasekhar J, Madura JD, Impey RW, Klein ML (1983) Comparison of simple potential functions for simulating liquid water. J Chem Phys 79(2):926–935
Jämbeck JPM, Lyubartsev AP (2012) Derivation and systematic validation of a refined all-atom force field for phosphatidylcholine lipids. J Phys Chem B 116(10):3164–3179
Kharakoz D, Colotto A, Lohner K, Laggner P (1993) Fluid-gel interphase line tension and density fluctuations in dipalmitoylphosphatidylcholine multilamellar vesicles: an ultrasonic study. J Phys Chem 97(38):9844–9851
Kharakoz DP, Shlyapnikova EA (2000) Thermodynamics and kinetics of the early steps of solid-state nucleation in the fluid lipid bilayer. J Phys Chem B 104(44):10368–10378
Kissinger HE (1957) Reaction kinetics in differential thermal analysis. Anal Chem 29(11):1702–1706
Klauda JB, Venable RM, Freites JA, OConnor JW, Tobias DJ, Mondragon-Ramirez C, Vorobyov I, MacKerell AD Jr, Pastor RW (2010) Update of the CHARMM all-atom additive force field for lipids: validation on six lipid types. J Phys Chem B 114(23):7830–7843
Kociurzynski R, Pannuzzo M, Böckmann RA (2015) Phase transition of glycolipid membranes studied by coarse-grained simulations. Langmuir 31:9379–9387
Kowalik B, Schubert T, Wada H, Tanaka M, Netz RR, Schneck E (2015) Combination of MD simulations with two-state kinetic rate modeling elucidates the chain melting transition of phospholipid bilayers for different hydration levels. J Phys Chem B 119(44):14157–14167
Krasikova IN, Khotimchenko SV, Solov'eva TF, Ovodov YS (1995) Mutual influence of plasmid profile and growth temperature on the lipid composition of *Yersinia pseudotuberculosis* bacteria. Biochim Biophys Acta Lipids Lipid Metab 1257(2):118–124
Leekumjorn S, Sum AK (2007) Molecular studies of the gel to liquid-crystalline phase transition for fully hydrated DPPC and DPPE bilayers. Biochim Biophys Acta Biomembr 1768(2):354–365
Leontiadou H, Mark AE, Marrink SJ (2004) Molecular dynamics simulations of hydrophilic pores in lipid bilayers. Biophys J 86(4):2156–2164
Lippert J, Peticolas W (1972) Raman active vibrations in long-chain fatty acids and phospholipid sonicates. Biochim Biophys Acta Biomembr 282:8–17
Mabrey S, Sturtevant JM (1976) Investigation of phase transitions of lipids and lipid mixtures by sensitivity differential scanning calorimetry. Proc Natl Acad Sci USA 73(11):3862–3866
MacKerell AD, Bashford D, Bellott MLDR, Dunbrack RL, Evanseck JD, Field MJ, Fischer S, Gao J, Guo H, Ha S, Joseph-McCarthy D, Kuchnir L, Kuczera K, Lau FTK, Mattos C, Michnick S, Ngo T, Nguyen DT, Prodhom B, Reiher WE, Roux B, Schlenkrich M, Smith JC, Stote R, Straub J, Watanabe M, Wiórkiewicz-Kuczera J, Yin D, Karplus M (1998) All-atom empirical potential for molecular modeling and dynamics studies of proteins. J Phys Chem B 102(18):3586–3616
Marrink SJ, Peter Tieleman D (2002) Molecular dynamics simulation of spontaneous membrane fusion during a cubic-hexagonal phase transition. Biophys J 83(5):2386–2392
Marrink SJ, Risselada J, Mark AE (2005) Simulation of gel phase formation and melting in lipid bilayers using a coarse grained model. Chem Phys Lipids 135(2):223–244
Mendelsohn R, Davies M, Brauner J, Schuster H, Dluhy R (1989) Quantitative determination of conformational disorder in the acyl chains of phospholipid bilayers by infrared spectroscopy. Biochemistry 28(22):8934–8939
Nagai T, Ueoka R, Okamoto Y (2012) Phase behavior of a lipid bilayer system studied by a replica-exchange molecular dynamics simulation. J Phys Soc Jpn 81(024):002
Nagle JF (1980) Theory of the main lipid bilayer phase transition. Annu Rev Phys Chem 31(1):157–196
Nagle J (1993) Arealipid of bilayers from NMR. Biophys J 64(5):1476
Nagle J, Scott H (1978) Lateral compressibility of lipid mono-and bilayers. Theory of membrane permeability. Biochim Biophys Acta Biomembr 513(2):236–243
Neuenfeld S, Schick C (2006) Verifying the symmetry of differential scanning calorimeters concerning heating and cooling using liquid crystal secondary temperature standards. Thermochim Acta 446(1):55–65
Parrinello M, Rahman A (1981) Polymorphic transitions in single crystals: a new molecular dynamics method. J Appl Phys 52(12):7182–7190
Picquart M, Lefévre T (2003) Raman and fourier transform infrared study of phytol effects on saturated and unsaturated lipid multibilayers. J Raman Spectrosc 34(1):4–12
Pluhackova K, Böckmann RA (2015) Biomembranes in atomistic and coarse-grained simulations. J Phys Condens Matter 27(32):323,103
Pluhackova K, Kirsch SA, Han J, Sun L, Jiang Z, Unruh T, Böckmann RA (2016) A critical comparison of biomembrane force fields: structure and dynamics of model DMPC, POPC, and POPE bilayers. J Phys Chem B 120(16):3888–3903
Qin SS, Yu ZW, Yu YX (2009) Structural characterization on the gel to liquid-crystal phase transition of fully hydrated DSPC and DSPE bilayers. J Phys Chem B 113(23):8114–8123
Riske KA, Barroso RP, Vequi-Suplicy CC, Germano R, Henriques VB, Lamy MT (2009) Lipid bilayer pre-transition as the beginning of the melting process. Biochim Biophys Acta Biomembr 1788(5):954–963
Sandoval-Perez A, Pluhackova K, Böckmann RA (2017) Critical comparison of biomembrane force fields: protein-lipid interactions at the membrane interface. J Chem Theory Comput 13:2310–2321
Schmitt T, Frezzatti W, Schreier S (1993) Hemin-induced lipid membrane disorder and increased permeability: a molecular model for the mechanism of cell lysis. Arch Biochem Biophys 307(1):96–103
Schrödinger LLC (2015) The PyMOL molecular graphics system, version 1.8
Schubert T, Schneck E, Tanaka M (2011) First order melting transitions of highly ordered dipalmitoyl phosphatidylcholine gel phase membranes in molecular dynamics simulations with atomistic detail. J Chem Phys 135(055):105
Siu SWI, Pluhackova K, Böckmann RA (2012) Optimization of the OPLS-AA force field for long hydrocarbons. J Chem Theory Comput 8(4):1459–1470

Steim JM, Tourtellotte ME, Reinert JC, McElhaney RN, Rader RL (1969) Calorimetric evidence for the liquid-crystalline state of lipids in a biomembrane. Proc Natl Acad Sci USA 63(1):104–109

Tardieu A, Luzzati V, Reman F (1973) Structure and polymorphism of the hydrocarbon chains of lipids: a study of lecithin-water phases. J Mol Biol 75(4):711–733

Tenchov B (1991) On the reversibility of the phase transitions in lipid-water systems. Chem Phys Lipids 57(2):165–177

Traeubl H, Sackmann E (1972) Crystalline-liquid crystalline phase transition of lipid model membranes. III. Structure of a steroid-lecithin system below and above the lipid-phase transition. J Am Chem Soc 94(13):4499–4510

Trudell JR (1977) A unitary theory of anesthesia based on lateral phase separations in nerve membranes. Anesthesiology 46(1):5–10

Tsuchida K, Ohki K, Sekiya T, Nozawa Y, Hatta I (1987) Dynamics of appearance and disappearance of the ripple structure in multilamellar liposomes of dipalmitoylphosphatidylcholine. Biochim Biophys Acta Biomembr 898(1):53–58

Tu K, Tobias DJ, Klein ML (1995) Constant pressure and temperature molecular dynamics simulation of a fully hydrated liquid crystal phase dipalmitoylphosphatidylcholine bilayer. Biophys J 69(6):2558

Vega C, Abascal JL (2011) Simulating water with rigid non-polarizable models: a general perspective. Phys Chem Chem Phys 13(44):19663–19688

Wiener M, Suter R, Nagle J (1989) Structure of the fully hydrated gel phase of dipalmitoylphosphatidylcholine. Biophys J 55(2):315–325